

Simulation of a scalar field on a fuzzy sphere

Fernando García Flores

Depto. de Física, Cinvestav, Apartado Postal 70-543, México D.F. 0730, MEXICO

Xavier Martin

*Université François Rabelais, Tours. Laboratoire de Mathématiques et Physique Théorique
CNRS, UMR 6083. Fédération de Recherche Denis Poisson (FR 2964)*

Denjoe O'Connor

School of Theoretical Physics, DIAS, 10 Burlington Road, Dublin 4, IRELAND

October 11, 2018

Abstract

The ϕ^4 real scalar field theory on a fuzzy sphere is studied numerically. We refine the phase diagram for this model where three distinct phases are known to exist: a uniformly ordered phase, a disordered phase, and a non-uniform ordered phase where the spatial $SO(3)$ symmetry of the round sphere is spontaneously broken and which has no classical equivalent. The three coexistence lines between these phases, which meet at a triple point, are carefully located with particular attention paid to the one between the two ordered phases and the triple point itself. In the neighbourhood of the triple point all phase boundaries are well approximated by straight lines which, surprisingly, have the same scaling. We argue that unless an additional term is added to enhance the effect of the kinetic term the infinite matrix limit of this model will not correspond to a real scalar field on the commutative sphere or plane.

1 Introduction

The fuzzy approximation scheme [1] consists in approximating the algebra of functions on a manifold with a finite dimensional matrix algebra and in principle provides a regularization of field theory on this space which can be used as an alternative to discretising the underlying space as is done in lattice field theory. Both the two-dimensional commutative [2] and Moyal planes can be viewed as the limits of a fuzzy sphere of infinite radius.

Here, we study a real scalar field, ϕ , with ϕ^4 interaction, in the fuzzy approach using Monte Carlo simulations. This becomes a Hermitian matrix model on the fuzzy sphere. The study reveals that the model has three distinct phases: (i) A disordered phase; (ii) a uniformly ordered phase and (iii) a non-uniformly ordered phase assimilated to a striped phase [3, 4, 5]. We find the collapsed phase diagram and in particular we calculate the uniform ordered/non-uniform ordered line that was absent in [6] and locate the triple point where the three phases meet. As the mass parameter varies, the non-uniformly ordered phase is absent for sufficiently small coupling, but as the coupling is increased this new phase opens up between the disordered and uniformly ordered phases. The three phases meet at a triple point.

The transition from the disordered to the non-uniformly ordered phase can also be identified with the one-cut to two-cut transition in matrix model theory [7, 8, 9]. This transition line merges with the predicted curve obtained from the quartic potential of the single trace pure matrix transition for sufficiently large couplings, i.e. sufficiently above the triple point. The qualitative features of the phase diagram are governed by this triple point. The presence of the non-uniformly ordered phase is the principal feature that distinguishes the phase diagram of the fuzzy model from its commutative counterpart.

A preliminary version of these results were presented in Lattice 05 and appeared in [10]. The principal aspects of these results have been confirmed in subsequent studies by Panero [11, 12] and Das et al. [13].

The current study could be relatively easily repeated for a Hermitian scalar field on other fuzzy spaces. The simplest extension would be to fuzzy $S^2 \times S^2$ or to fuzzy CP^N [14]. Fuzzy versions of S^3 and S^4 are also accessible [15] and will hopefully be studied in the near future. In all cases, the structure of the phase diagram should be similar, although there is no guarantee that all coexistence lines will collapse with a consistent scaling as happens for the two dimensional sphere. One prediction for the general case is that the disordered non-uniformly ordered line will always be present for sufficiently large coupling and will again merge with the pure one-cut two-cut transition for the pure matrix model.

In section 2 we review the construction of the fuzzy sphere and in section 3 we present the model, section 4 describes the Metropolis algorithm, section 5 studies limiting models such as the lowest matrix size (two by two) and the pure matrix model, section 6 describes the observables and simulations, particularly the specific heat which we use to locate transitions. Section 7 gives our main results and describes the collapsed phase diagram and locates the triple point. Section 8 gives our conclusions. The paper ends with some technical appendix for the optimization of the simulations.

2 The fuzzy sphere

Before introducing the fuzzy sphere, let us look at some basic properties of the *ordinary continuum 2-sphere*. A 2-sphere centered on the origin, with radius R , embedded in \mathbb{R}^3 , denoted simply \mathbb{S}^2 , can be defined as the set of points (x_1, x_2, x_3) in \mathbb{R}^3 such that $x_1^2 + x_2^2 + x_3^2 = R^2$. It can also be expressed by the angles (ϑ, φ) of spherical coordinates.

Taking two elements of the algebra, $f(\vartheta, \varphi)$ and $g(\vartheta, \varphi)$, we define their *inner product* as

$$\langle f|g \rangle = \int_{\mathbb{S}^2} d\Omega f^*(\vartheta, \varphi) g(\vartheta, \varphi), \quad (1)$$

and their *norm* as

$$\|f\|^2 = \langle f|f \rangle = \int_{\mathbb{S}^2} d\Omega |f(\vartheta, \varphi)|^2. \quad (2)$$

where $\int_{\mathbb{S}^2} d\Omega = \int_0^{2\pi} d\varphi \int_0^\pi d\vartheta \sin(\vartheta)$. The norm must be finite for any element of the algebra (square integrable functions). Both equations, (1) and (2), define the *Hilbert space* \mathcal{H} which allows us to quantize the theory.

In general, the *Laplace operator* contains information on the geometry of the space, *i.e.* it depends on the metric as $\nabla^2 = \frac{1}{\sqrt{|g|}} \partial_i \sqrt{|g|} \partial^i$, where g is the determinant of the metric tensor $g_{\mu\nu}$ on Riemannian and pseudo-Riemannian manifolds [16]. In particular, the Laplacian on the sphere is $\nabla^2 = \frac{1}{(R \sin \vartheta)^2} \frac{\partial^2}{\partial \varphi^2} + \frac{1}{R^2 \sin \vartheta} \frac{\partial}{\partial \vartheta} \left(\sin \vartheta \frac{\partial}{\partial \vartheta} \right)$. The eigenfunctions of this operator are the spherical harmonics $Y_{\ell m}(\vartheta, \varphi)$ with $\ell = 0, 1, 2, \dots$ and $m = -\ell, -(\ell-1), \dots, (\ell-1), \ell$ which come as solutions of the Helmholtz equation $\Delta f + l(l+1)f = 0$ on the unit sphere.

A convenient basis to describe any function on the sphere is given by these *spherical harmonics* $Y_{\ell m}(\vartheta, \varphi)$ since they form a complete set of orthonormal functions and thus, any square-integrable function can be expanded as a linear combination of these.

$$f(\vartheta, \varphi) = \sum_{\ell=0}^{\infty} \sum_{m=-\ell}^{+\ell} c_{\ell m} Y_{\ell m}(\vartheta, \varphi), \quad (3)$$

N	R	Θ	Limit
N_0	R_0	$\frac{2R^2}{\sqrt{N^2-1}}$	Fuzzy sphere (\mathbb{S}_F^2)
$+\infty$	R_0	0	Commutative sphere (\mathbb{S}^2)
$+\infty$	$+\infty$	0	Commutative plane (\mathbb{R}^2)
$+\infty$	$+\infty$	Θ_0	Moyal plane

Table 1: Some spaces as limits of the fuzzy sphere.

where the orthonormalization condition

$$\int_{\mathbb{S}^2} d\Omega Y_{\ell m}^*(\vartheta, \varphi) Y_{\ell' m'}(\vartheta, \varphi) = \delta_{\ell\ell'} \delta_{mm'}, \quad (4)$$

allows us to compute the $c_{\ell m}$ coefficients as

$$c_{\ell m} = \int_{\mathbb{S}^2} d\Omega Y_{\ell m}^*(\vartheta, \varphi) f(\vartheta, \varphi). \quad (5)$$

We are now ready to define the *fuzzy sphere* \mathbb{S}_F^2 of radius R [17, 18, 19]. It is a non-commutative space defined in terms of the $N \times N$ matrix operators $(\hat{x}_1, \hat{x}_2, \hat{x}_3)$ subject to the relations

$$\hat{x}_1^2 + \hat{x}_2^2 + \hat{x}_3^2 = R^2 \hat{1}, \quad \text{and} \quad [\hat{x}_i, \hat{x}_j] = i\varepsilon_{ijk} \frac{2R}{\sqrt{N^2-1}} \hat{x}_k = i\varepsilon_{ijk} \Theta \frac{\hat{x}_k}{R}, \quad (6)$$

with $\Theta = 2R^2/\sqrt{N^2-1}$ and ε_{ijk} the totally antisymmetric unit tensor. The operators \hat{x}_i can be related to the angular momentum operators \hat{L}_i in their irreducible representation of $SU(2)$ of size $(2\ell+1)$ with the formula

$$\hat{x}_i = \frac{2R}{\sqrt{N^2-1}} \hat{L}_i = \frac{\Theta}{R} \hat{L}_i, \quad (7)$$

where the relation between the matrix size N and the representation of the angular momentum ℓ is given by $N = 2\ell + 1$. Replacing the equation (7) in (6) we recover the angular momentum algebra.

In the table 1 we show some limits of the fuzzy sphere in terms of the matrix size N and the radius of the sphere R . In that way, the fuzzy sphere contains some other spaces as limits of the matrix size and its radius.

From the algebra of matrices of size N , denoted Mat_N , generated by the position operators \hat{x}_i in (6), one can define a *Hilbert space*, by introducing an *inner product*. To do that, consider two elements of the algebra Mat_N denoted ϕ and ψ , their scalar product and associated *norm* are defined by

$$\langle \phi | \psi \rangle = \frac{4\pi}{N} \text{Tr} [\phi^\dagger \psi], \quad \|\phi\|^2 = \langle \phi | \phi \rangle = \frac{4\pi}{N} \text{Tr} [\phi^\dagger \phi], \quad (8)$$

where the normalization was chosen so that the unit matrix $\hat{1}$ and the constant function 1 on the sphere have the same norm.

The geometry of the spaces is given through derivation operators. In the case of \mathbb{S}_F^2 , the derivations \mathcal{L}_i correspond to the adjoint action $[\hat{L}_i, \cdot]$ of the angular momentum operators \hat{L}_i of $SU(2)$. The Laplacian is then deduced as

$$\mathcal{L}^2 \phi = \mathcal{L}_i \mathcal{L}_i \phi = [\hat{L}_i, [\hat{L}_i, \phi]]. \quad (9)$$

Similar to the expansion (3) of a function $f(\vartheta, \varphi)$ on \mathbb{S}^2 , a convenient basis to expand any $N \times N$ matrix ϕ on \mathbb{S}_F^2 is the *polarization tensor* basis. The polarization tensors are denoted by $\hat{Y}_{\ell m}$ with $0 \leq \ell \leq (N-1)$ and $-\ell \leq m \leq +\ell$, and are defined as the simultaneous eigenvectors of the laplacian \mathcal{L}^2 and axial angular momentum \mathcal{L}_3 :

$$\mathcal{L}^2 \hat{Y}_{\ell m} = \ell(\ell+1) \hat{Y}_{\ell m}, \quad \mathcal{L}_3 \hat{Y}_{\ell m} = m \hat{Y}_{\ell m}, \quad (10)$$

and we see that \mathcal{L}^2 is a cut-off version of $-\nabla^2$. They are normalised to form an orthonormal basis of Mat_N

$$\frac{4\pi}{N} Tr [\hat{Y}_{\ell m}^\dagger \hat{Y}_{\ell' m'}] = \delta_{\ell \ell'} \delta_{m m'}, \quad (11)$$

and transform simply under complex conjugation

$$\hat{Y}_{\ell m}^\dagger = (-1)^m \hat{Y}_{\ell -m}. \quad (12)$$

The expansion of ϕ in $\hat{Y}_{\ell m}$ is given by

$$\phi = \sum_{\ell=0}^{N-1} \sum_{m=-\ell}^{+\ell} c_{\ell m} \hat{Y}_{\ell m}, \quad (13)$$

where the coefficients can be computed by means of the orthonormality condition

$$c_{\ell m} = \frac{4\pi}{N} Tr [\hat{Y}_{\ell m}^\dagger \phi]. \quad (14)$$

3 Real scalar field on a fuzzy sphere

Before introducing the real scalar field theory on the fuzzy sphere, let us look at this theory on an ordinary continuum 2-sphere.

Let ϕ be a real scalar field on a sphere \mathbb{S}^2 with radius R and ϕ^4 potential, the functional action is given as

$$S[\phi] = \int_{\mathbb{S}^2} d\Omega \left[\frac{1}{2} (\nabla \phi)^2 + \frac{1}{2} r R^2 \phi^2 + \frac{1}{4!} \lambda R^2 \phi^4 \right], \quad (15)$$

where ∇_i ($i = 1, 2, 3$) are the usual generators of rotations, r is the *mass parameter* and λ is the *coupling constant* which may depend on the radius of the sphere.

Second order phase transitions can not appear in finite volume systems, such as the sphere. However, it becomes possible in the *planar limit*, $R \rightarrow \infty$. The ϕ^4 model on a bidimensional plane, which corresponds to the planar limit of the sphere, is defined by the action

$$S[\phi] = \int_{\mathbb{R}^2} d^2\mathbf{x} \left[\frac{1}{2} (\nabla\phi)^2 + \frac{1}{2} r\phi^2 + \frac{1}{4!} \lambda\phi^4 \right].$$

This model has been widely studied, see for example [20, 21].

Similarly, the model to study on the fuzzy sphere is a *Hermitian matrix model* which corresponds to a real scalar field and is given by the action [6, 22]

$$S[\phi; N, a, b, c] = \text{Tr} \left[a [\hat{L}_i, \phi]^\dagger [\hat{L}_i, \phi] + b\phi^2 + c\phi^4 \right] = \text{Tr} \left[a\phi^\dagger (\mathcal{L}^2\phi) + b\phi^2 + c\phi^4 \right], \quad (16)$$

where N is the size of the matrix, b is the real *mass parameter*, and c is the real, positive, *coupling constant*. Similarly to a commutative sphere, $[\hat{L}_i, \cdot]$ are the usual rotation generators where \hat{L}_i is the *angular momentum operator* in its irreducible representation of $SU(2)$ with size $N = (2\ell + 1)$ defined by the commutation relations $[\hat{L}_i, \hat{L}_j] = \varepsilon_{ijk} \hat{L}_k$. The constant a is a positive number employed to fix the units¹. The a term, called *kinetic term*, contains the information on the geometry of the space by means of the Laplacian, while the rest of the action is called *potential term* and denoted $V(\phi)$.

The action (16) approximates the continuum action (15) when

$$a = \frac{2\pi}{N}, \quad b = \frac{2\pi r R^2}{N}, \quad c = \frac{\pi \lambda R^2}{6N}. \quad (17)$$

These parameters are chosen so that the fuzzy action was normalised so that $S[\hat{\mathbf{1}}]$ for the unit function/matrix be the same on the continuum and fuzzy sphere.

The absolute minima of this action can be obtained by searching for configurations minimizing both the kinetic and potential term *separately*. The kinetic term is obviously positive and is therefore minimum when $\mathcal{L}^2\phi = 0$, that is when $\phi = \alpha\hat{\mathbf{1}}$ is proportional to the identity. Replacing this constraint in the potential term, we get

$$V(\alpha\hat{\mathbf{1}}) = N(b\alpha^2 + c\alpha^4). \quad (18)$$

The necessary conditions to have a minimum are: $S'(\bar{\alpha}) = 0$ and $S''(\bar{\alpha}) > 0$. If $b < 0$ then we find two absolute minima at

¹It is possible to scale ϕ , b and c to absorb a i.e. fit a to one. The scaling for the field is given by: $\phi = \psi/\sqrt{a}$, leading to a scaling for the other parameters of $\tilde{b} = b/a$, and $\tilde{c} = c/a^2$. These changes affect the expectation values by a constant overall scaling which has no consequence on such things as phases and phase boundary lines.

$$\bar{\alpha} = \pm\alpha_0 = \pm\sqrt{\frac{-b}{2c}}, \quad (19)$$

which have energy $S(\bar{\alpha}) = -Nb^2/4c$, whereas when $b > 0$ there is only one minimum at $\bar{\alpha} = 0$. Finally, when $b = 0$, there is a critical point at $\bar{\alpha} = 0$ which is clearly a minimum since $S(\alpha) = Nc\alpha^4$ and $c > 0$.

There are however other *local minima* to this action which will play an important role in one of the phases of this model. They can be located approximately by looking at the minima of the potential [6] which are given by $U^\dagger DU$ where U is a unitary matrix and D a diagonal matrix with diagonal elements $\pm\alpha_0$. The absolute minima found above correspond to the particular case when all the diagonal entries of D are identical.

4 The Metropolis simulation

We started the simulations by using a standard Metropolis Monte Carlo algorithm [24, 25] with the jackknife estimator for the error [26] to account for the autocorrelation of the samples..

The *initial conditions*, *i.e.* the choice of the first configuration in the Markov chain can be of two types: *Cold initial conditions*, which correspond to configurations which are classical minima of the action, or *Hot initial conditions*, which are configurations chosen randomly in the phase space. We made sure in our numerical simulations that none of our results depended on the initial conditions, whether they were cold or hot.

In general, when we start the simulation the sequence of samples obtained by Metropolis algorithm goes through a transient regime where it does not obey the desired statistics yet. This is the *thermalization process*. This is true even in the case of “cold” initial conditions because the classical minima may be probabilistically irrelevant when the fluctuations are important. This actually happens in one of the phases of our model (the non-uniform ordered phase).

Tunneling is an essential process in our model as there are multiple classical minima which contribute significantly to the probability distribution of the field. Typically, tunneling is exponentially suppressed by the energy barrier separating the classical minima. It can therefore be difficult to account for in the Monte-Carlo algorithm. To improve the probability of tunneling, we have tried various sampling methods.

The two simplest ways of sampling the phase space are to either make a big change on the matrix as a whole or to perturb its entries one by one. The first method allows for big changes and helps tunneling but usually yields unfavored, high energy, test configurations which are rejected and in-

crease the autocorrelation between configurations. On the other hand, the latter is good at exploring the phase space locally, but has a low chance of tunneling. Even alternating the two methods to enjoy both their advantages is not sufficient to produce the tunneling necessary in the model studied.

As we already discussed at the end of section 3, the classical minima of the action are located at $\pm\sqrt{-b/2c}$. Thus, the interval where we must vary the real and imaginary part of every entry of the matrix during the sampling should be about $I = [-2\sqrt{-b/2c}; 2\sqrt{-b/2c}]$. In practice, we have found empirically that we need an interval of variation of the field between 2.3 and 2.6 times bigger.

When we use an interval less than $2.3I$, the trace effective probability density distributions of the matrix will not reproduce the results obtained via direct integration for $N = 2$. In general, this effect also appears for any matrix size N . The upper bound does not affect the results so much as the auto-correlation of samples (more configurations are rejected by the metropolis algorithm) and thus the speed of convergence of the code. We have found that $2.6I$ is the optimum upper bound to balance speed and precision.

A more sophisticated method we have successfully implemented is the *annealing method* [25]. The idea is to produce favored decorrelated test configurations by introducing a temperature-like parameter β in the probability distribution $\exp(-\beta S)$. The Metropolis sampling is done normally with $\beta = 1$. During that sampling, the field is typically trapped around one of the classical minima. Periodically, the Metropolis sampling is interrupted, and this parameter is lowered (*i.e.* the temperature is increased) which smoothes out the action and allows the field to move more freely between the classical minima. Then β is raised back to one (*i.e.* the temperature is lowered back) trapping the field around a classical minimum which is hopefully decorrelated from the previous one.

The annealing method thus increases the probability of tunneling between minima of the action and decreases the autocorrelation between configurations. It also increases the computation time, but the gain in efficiency is largely dominant, making this method very useful and reliable for simulations with larger matrices.

The computation time can still be too large, making the simulation impossible to run in practice. We have developed a method where the real time of computation decreases dramatically which we present in the appendix.

5 Limiting models

In this section we present the lowest dimensional model which can be integrated directly and the pure potential model which can be solved analytically. They will both be useful to test the validity of our Monte-Carlo simulation in some particular limits.

5.1 Lowest dimensional model

It is quite useful to investigate the lowest dimensional model ($N = 2$) as it has only two independent parameters and can therefore be well understood, and integrated directly. This provides a good independent computation to test our Monte-Carlo code against. Furthermore, it happens that even this low dimensional case shows all the features of the large N limit!

In the simplest case $N = 2$, the action (16) can be simplified by expanding the field in terms of an orthonormal basis $\{\mathbf{1}, \sigma_k\}$, where $\mathbf{1}$ is the 2×2 identity matrix and σ_k are the three *Pauli matrices*. The expansion is

$$\phi = \alpha \mathbf{1} + \vec{\rho} \cdot \vec{\sigma} \quad (20)$$

where the coefficients α and ρ_k are in \mathbb{R} . Then, writing down the action (16) in terms of this new set of variables, we get

$$S = 4a\rho^2 + 2b(\alpha^2 + \rho^2) + 2c(\alpha^4 + 6\alpha^2\rho^2 + \rho^4) \quad (21)$$

where ρ is the norm of $\vec{\rho}$.

The action (21) depends only on the modulus of the vector $\vec{\rho}$. This property allows us to integrate out the degrees of freedom associated with the *rotational symmetry* of the vector $\vec{\rho}$, which is the expression of the general $SU(2)$ symmetry of the action in two dimensions. The corresponding effective probability density distribution is given by

$$P_{\text{eff}}[\alpha, \rho] = \frac{1}{Z} \rho^2 e^{-S[\alpha, \rho]} = \frac{1}{Z} e^{-S_{\text{eff}}[\alpha, \rho]}, \quad Z = \int d\alpha d\rho \rho^2 e^{-S} = \int d\alpha d\rho e^{-S_{\text{eff}}}, \quad (22)$$

where $S_{\text{eff}} = S - \ln \rho^2$ is the associated effective action.

This simple example depends on two variables only, which makes it possible to integrate numerically without a lot of effort for any set of parameters $\{a, b, c\}$ via the trapezoidal rule or any other algorithm [27], to get the expectation values. In this sense, *we can solve directly the model for any set of parameters making it possible to test our Monte Carlo code*. Any graph in this section will not include error bars because, with direct integration, they are negligible.

Because of the $SU(2)$ symmetry of the theory, the expectation values of $\langle |\alpha| \rangle$ and $\langle \rho \rangle$ give us the whole information about the average configuration $\langle \phi \rangle$. We can see their behavior in the figure 1, computed from a direct integration with $N = 2$, $a = 1$, and for a typical value of $c = 50$, as a function of the remaining parameter b of the model (scaled to $bc^{-1/2}$). We can see three distinct phases:

1. *Disordered phase*: the expectation values of $|\alpha|$ and ρ are close to zero, roughly in the interval $(0, +\infty)$.
2. *Uniform ordered phase*: the most important contribution to the configuration is given by the expectation value of α , roughly in the interval $(-\infty, -24)$

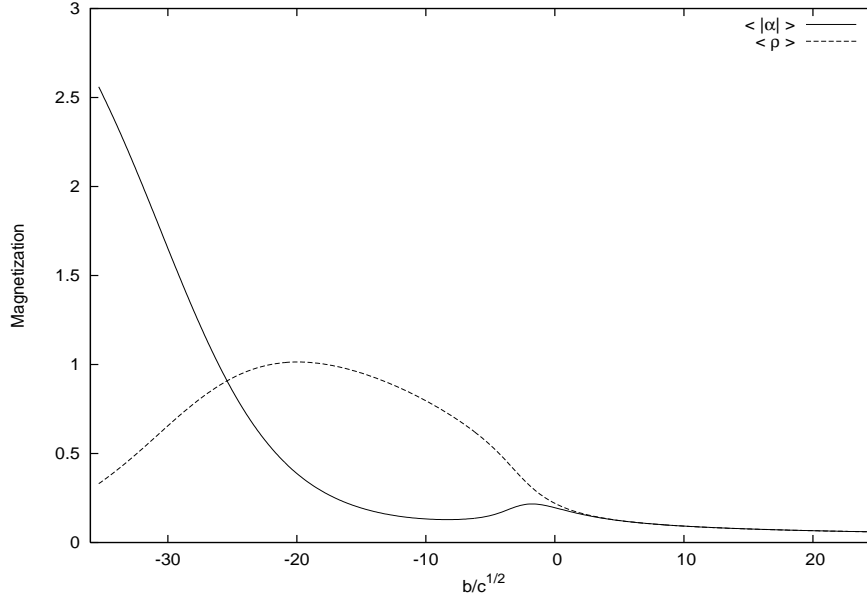


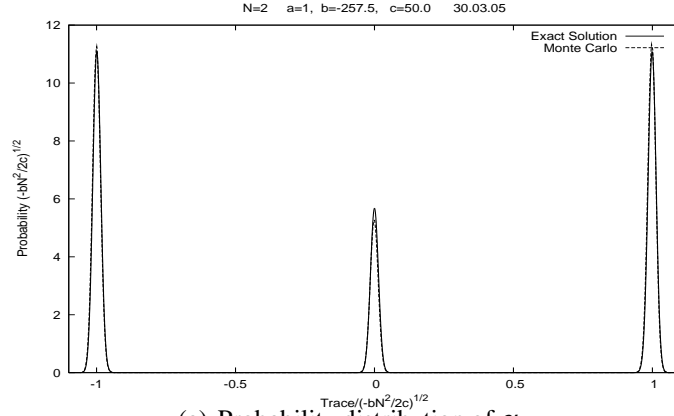
Figure 1: Expectation value of $|\alpha|$ and ρ obtained from direct numerical integration.

3. *Non-uniform ordered phase*: the system is ordered but the main contribution to the configuration is given by the expectation value of ρ , in between the previous two phases.

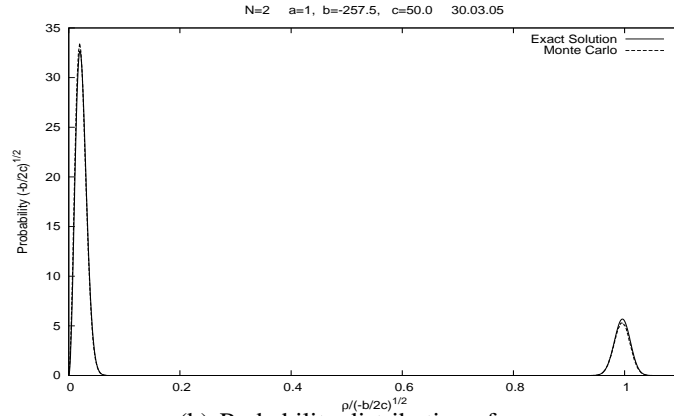
The disordered phase has averages of $|\alpha|$ and ρ , in the expansion (20), at approximately 0 and the typical configuration is thus distributed around zero. This phase is analogous to the *paramagnetic phase* in ferromagnetic materials. Following the analogy, if we take the parameter b as a “*temperature parameter*”, the thermal fluctuations do not allow any kind of ordering in the material when the temperature is bigger than some critical value. The thermal fluctuations are getting stronger and stronger when the temperature is increased.

The uniform ordered phase is characterized by the fact that the most important contribution to the configurations is given by the coefficient α , in the expansion (20). The expectation value of ρ is negligible with respect to the expectation value of $|\alpha|$. This means that the configuration is approximately proportional to the identity matrix. This phase is analog to the *magnetic phase*, in ferromagnetic materials.

In the third and last phase (the non-uniform ordered phase), both $|\alpha|$ and ρ contribute to the configuration but in this region of the parameter space, ρ is more important than $|\alpha|$. This phase has ordering *i.e.* the field has non-zero expectation value but this ordering is not an analog of any ferromagnetic ordering. It was argued in [11, 12] that in this phase, the eigenvalues of the matrix has two cuts located at the two minima of the action $\pm\alpha_0$ given in (19), whereas [6] speculated that



(a) Probability distribution of α .



(b) Probability distribution of ρ .

Figure 2: Comparison of the unnormalised probability density distributions of some observables for $N = 2$. In most cases, the two curves cannot be distinguished.

the eigenvalues of ϕ would be split equally between positive and negative eigenvalues. For $N = 2$, it means trivially that $\phi = \alpha_0 \sigma_3$ up to a free $SU(2)$ rotation, and thus one would expect $\langle |\alpha| \rangle \ll \alpha_0$ and $\langle \rho \rangle \simeq \alpha_0 = \sqrt{-b/c^{0.5}}/(4c)^{0.25}$. This is indeed true in figure 1, as for $-20 < b/\sqrt{c} < -5$, $\langle \rho \rangle$ does curve like $\sqrt{-b/c^{0.5}}/200^{0.25} \simeq \sqrt{-b/c^{0.5}}/4$ and is much bigger than $\langle |\alpha| \rangle$.

As stated earlier, we can also use the results from this alternate method to validate the Monte-Carlo code for $N = 2$. The figure 2 shows the unnormalised effective probability density distributions of the quantities α and ρ . In that case, we can compare directly both effective probability density distributions. The excellent agreement shows that the statistical error bars are negligible, but the most important thing is that the program has sampled the phase space properly. We have already checked many points in the parameter space and we have always obtained identical results up to error bars.

At the moment, we have shown the convergence of our simulation in the *lowest dimensional model*, but our goal is of course focused on simulating the model using bigger matrix sizes to extrapolate to the *continuum limit* ($N \rightarrow +\infty$). Still we will see that the $N = 2$ results are already remarkably good approximations of the large N limit.

5.2 Pure potential model

The *pure potential model* interests us for two reasons: it can be solved analytically and gives a good approximation for the transition curve between the disordered and non-uniform ordered phases discussed previously [6]. It comes from setting $a = 0$ in the action (16), only keeping what we called the potential term. This approximation is increasingly accurate as the transition is tracked to larger couplings far from the triple point.

This model ($a = 0, N \rightarrow \infty$) has been solved by many authors [28, 29]. In term of their solution we can get an expression of the specific heat and other thermodynamics quantities which are a good reference to compare to the numerical results and the convergence of the algorithm when we increase N .

The specific heat in this approximation has the form

$$C_V = \begin{cases} \frac{1}{4} & \bar{\tau} < -1 \\ \frac{1}{4} + \frac{2\bar{\tau}^4}{27} - \frac{\bar{\tau}}{27} (2\bar{\tau}^2 - 3) \sqrt{\bar{\tau}^2 + 3} & \bar{\tau} > -1 \end{cases} \quad (23)$$

where $\bar{\tau} = b/|b_c|$ with $b_c = -2\sqrt{Nc}$ is the critical mass. From equation (23) the phase transition is a third order transition because the first derivative of the specific heat has a finite discontinuity in $\bar{b} = -1$.

Another way to detect the phase transition is to look at the probability distribution of the field eigenvalues. In the disordered phase, they are confined into a single connected region centered around zero, whereas in the non-uniform ordered phase, they are split into two disconnected regions centered respectively around $\pm\sqrt{-b/2c}$ corresponding to the minima of the polynomial potential. Due to this characteristic behaviour, we also refer to this as a “one cut–two cut” transition. We will also use this terminology for the disorder/non-uniform transition since the work of Panero [11, 12] shows that the transition in the fuzzy sphere model, where $a \neq 0$, also have this characteristic behaviour.

The phase boundary for this model is given by

$$b = -2\sqrt{Nc} \quad (24)$$

and is included in the phase diagram shown in figure 6 at the end of this article.

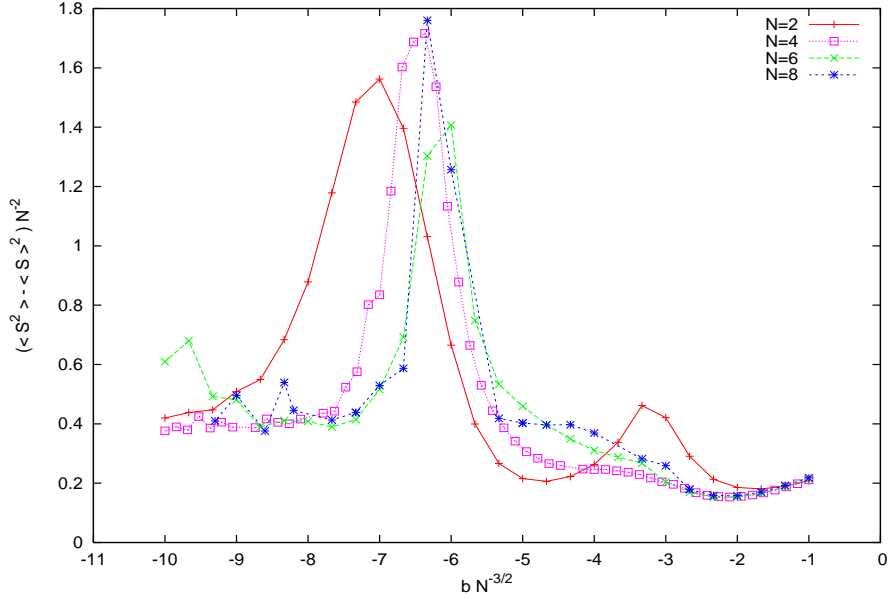


Figure 3: Specific heat for $a = 1$ and $c = 40$.

6 Observables and Simulations

For the model under study, the number of degrees of freedom is N^2 , which corresponds to the number of independent real entries in a Hermitian matrix. Thus, the thermodynamic limit we are interested in corresponds to matrices of infinite size. The standard procedure, to take the thermodynamic limit, is to define a scaling of the parameters of the model such that the relevant observables collapse in a phase diagram independent of the matrix size. If the phase diagram collapses in a reasonable way, then we can straightforwardly extrapolate it to the thermodynamic limit.

The specific heat is a measure of the dispersion of the energy. It is sensitive to the phase transitions which register as peaks in it. We therefore use it as the order parameter. Typically, it will present one or, more often, two peaks as we show in figure 3 for $\{a = 1, c = 40\}$ and various matrix sizes. The very obvious peak is located around $bN^{-3/2} = -6 \pm 0.4$, the other one, almost imperceptible is around $bN^{-3/2} = -3$. For the biggest matrix size investigated $N = 10$, simulations for a curve as the one in figure 3 took about a day. The error bars provided by the jackknife algorithm were omitted as they are quite small and would only crowd the figure more.

Other observables, such as $\langle \text{Tr}[\phi^2] \rangle$ and $\langle |\text{Tr}[\phi]| \rangle$ which were used as order parameters in [6], their susceptibilities, and the internal energy $\langle S \rangle$ have also been collected but are not shown here. They will be used in section 7 to identify the phases though.

It is an important remark that the transition, from the non-uniform ordered phase to the uniform ordered phase, presents a very high and wide peak in the susceptibilities which can subsume and hide the smaller one when near the triple point, making it impossible to determine its exact position. As a result, the data points of this transition curve in the phase diagram could not be found near the triple point. However, Panero [11], by looking at the eigenvalue distribution of ϕ for $c/aN^2 = 1/2$ provides an additional point on this curve very near the triple point.

In the figure 3, the scaling for b , given by $bN^{-3/2}$, which aligns the peaks (and thus the location of the phase boundary) for different matrix sizes has already been included. It is remarkable that with this scaling, the $N = 2$ curve has the same qualitative behavior as the $N = 10$ curve, as announced previously, but the peak in figure 3, is already a reasonable approximation of the large N limit peak found for $N = 10$.

This analysis was repeated for a wide range of the parameter c and for matrix sizes $N \leq 10$. The collected results, the interpretation of the phases and the collapsed phase diagram will be presented in section 7.

7 Results

In this section, we will present the collapsed phase diagram as well as an analysis of the three phases observed.

In the plots 4 and 5, we can see different profiles of the probability density distributions as a function of the mass parameter b for $\text{Tr}[\phi]$ and $\rho = \sqrt{|c_{1-1}|^2 + |c_{10}|^2 + |c_{11}|^2}$ which gives the power in the $l = 1$ angular momentum mode in (13), with $\{a = 1, c = 40, N = 4\}$. There, we can appreciate the three different phases of the model.

In the uniform order phase, for b negative enough, the trace is distributed around two symmetric values centered on $\pm\alpha_0$ respectively,² and ρ is distributed close to zero, *i.e.* it gives no contribution to the typical configuration. In this phase, ϕ is approximately proportional to the unit matrix and the rotational symmetry is thus preserved.

The non-uniform ordered phase, for intermediate values of b , has the peculiarity that the most exterior peaks of the probability of the trace, which correspond to the absolute minimum of the action $\pm\alpha_0$ and thus to the field in the uniform order phase, are smaller than the new peaks which arise between them. Furthermore, the most probable value of ρ is not close to zero. In this phase, the power of the configuration is thus in higher angular momentum modes (as defined in the expansion

² α_0 was defined in (19) as the location of the absolute minimum of the action.

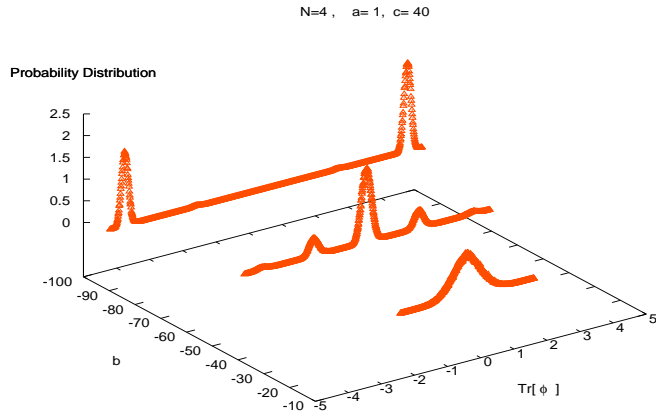


Figure 4: Probability distribution of the trace of ϕ as a function of b

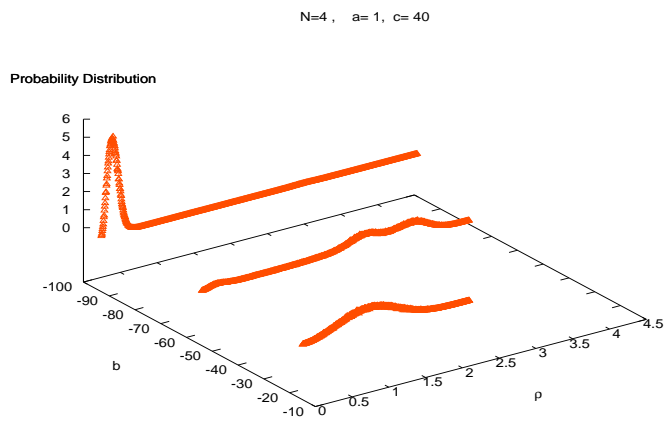


Figure 5: Probability distribution of ρ as a function of b .

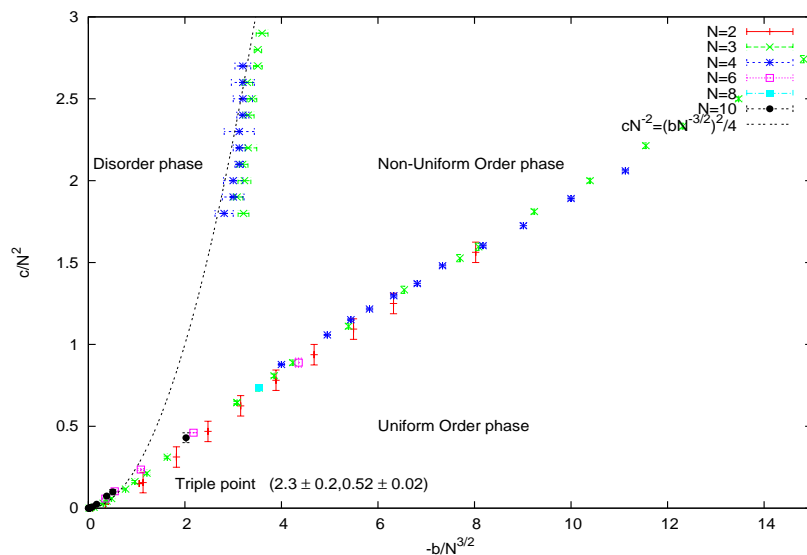


Figure 6: Full collapsed phase diagram.

(13) in polarization tensors) and the rotational symmetry has been spontaneously broken.

The last curve is representative of the disordered phase. In this phase the configurations (both the trace and ρ) are spread over a long interval but very close to zero restoring the rotational symmetry.

A phase diagram is a map that contains the thermodynamics or physical properties of a given system. This implies that, to construct a phase diagram, we need quantities in the thermodynamic limit. As explained in section 6, this is done by finding a scaling in the bare parameters of the model, b and c here, to make it independent of the number of degrees of freedom N .

We had already found in section 6 that the scaling necessary to make the diagram independent of N was $N^{-\frac{3}{2}}$ for the mass parameter b . Repeating the simulations for various values of c and plotting the phase boundaries found for all values of N simulated, we found a scaling in N^{-2} for the coupling constant c . This scaling is the same for *all* the coexistence curves which guarantees a consistent $N \rightarrow \infty$ limit. We can then define scale-free parameters

$$\bar{b} = \frac{b}{aN^{3/2}}, \quad \bar{c} = \frac{c}{a^2N^2}. \quad (25)$$

Remember that for all the simulations and results in this paper, we have set $a = 1$.

These results are presented in the figure 6 which shows the phase diagram for the ϕ^4 model on a fuzzy sphere. The three phases we identified above are delimited by the coexistence curves which meet at a triple point. These coexistence curves can be fitted to get an algebraic expression for each one of them using the scale-free parameters introduced above in (25)

As mentioned in section 6 we could not access the Disorder/non-uniform order phase boundary near the triple point. However since the curve is consistent with a straight line, we can extrapolate it to the triple point without any difficulty. We find:

$$\text{Disorder/non-uniform order: } \bar{c} = 2.29(-\bar{b}) - 4.74. \quad (26)$$

As expected, for large \bar{c} , this curve is well approximated by the one obtained for the pure potential model derived in 5.2, given in scale-free parameters by

$$\bar{c} = (-\bar{b})^2/4, \quad (27)$$

and drawn with a dashed line in the phase diagram, figure 6.

We did not focus on the disorder/uniform order boundary line in this paper since it has already been studied in detail in [6]. It was found there to be a straight line going through the origin. Converting its equation to our scale-free parameters through (25), we get

$$\text{Disorder/uniform order: } \bar{c} = 0.23(-\bar{b}). \quad (28)$$

Finally, the uniform-non-uniform order phase boundary line which was studied in detail in this paper is approximately straight with equation

$$\text{Uniform - non-uniform order: } \bar{c} = 0.2(-\bar{b}) + 0.07 \quad (29)$$

which just prolongs the disorder/uniform order line, up to error bars.

These three coexistence curves, (26,28,29), intersect at a triple point given by

$$(\bar{b}_T, \bar{c}_T) = (-2.3, 0.52). \quad (30)$$

These values are consistent with the data presented in [11]. In fact, figures (11-30) there correspond precisely to $\bar{c} = 0.5 \simeq \bar{c}_T$, and by identifying the point where the eigenvalue density undergoes the one cut-two cut transition described in section 5.2, one finds that his data gives $\bar{b}_T \simeq 2.3$ consistently for $N = 15, 17, 19, 21, 23$.

If instead one takes the asymptotic form of the disorder non-uniform order transition line given by the one cut-two cut transition (27) instead of (26), and finds its intersection with the disorder-uniform order transition curve (28), the triple point occurs at

$$(\bar{b}_T^e, \bar{c}_T^e) = (-0.92, 0.21). \quad (31)$$

We conclude from this that the effect of the kinetic term is to move the triple point to larger values along the line governing the disorder/uniform order transition.

8 Conclusions

In the main part of the paper, we presented the results for the numerical simulation by means of an optimized Metropolis algorithm for the ϕ^4 matrix model. In the appendix we develop the metropolis algorithm which makes more efficient the simulation of matrix models. In particular, we argue that the algorithm proposed presents considerable advantages with respect to the usual Metropolis algorithm in the simulation of matrix models [30]. The reduction in the processing time for both non-uniform ordered and uniform ordered phases will be more evident for large matrices and, of course, when we are far away from the coexistence curves due to the fact that the minima of the potential are more separated. A different approach was used with equal success in [11].

Figure 6 shows the phase diagram for the model given by (16) and refines the phase diagram which was incomplete in [6]. The data have been collapsed using the scaling form shown on the axis and defined in (25). It is consistent with the scaling of the exact solution of the pure matrix model which only fixed the quotient of the two scalings. One of the important features of the diagram is that all three coexistence lines can be collapsed simultaneously. This did not have to happen and in fact the corresponding lines do not all collapse together for a related three dimensional model [31], where the spacetime is taken to be a fuzzy sphere direct producted with a temporal direction.

This diagram contains the information about three different phases, the well known disordered and uniform ordered phase, and a new phase, the non-uniformly ordered phase (where the $SO(3)$ spatial symmetry of the round sphere is spontaneously broken), as well as the scaling of the model, and the coexistence curves. We could even estimate the coordinates of the triple point which is the point where the three phases coexist in equilibrium. The coordinates of this triple point are consistent with the independent simulation [11].

Another article [13] finds different results, including an extra phase and no scaling. An obvious reason may be that in the phase diagram they show for $N = 25$, our scale-free parameter $-\bar{b}$ has a very small range in our scale-free parameters of $[0;0.13]$, meaning it only shows a tiny corner of our phase diagram of figure 6. Furthermore, they use the probability distribution of ϕ_{11} (denoted Φ_{11} there) as an observable to detect the transition between the two ordered phases. First, this does not seem to be a physically meaningful observable, especially given the $SU(2)$ symmetry of the model. Furthermore, they obtain a curve somewhat similar to the one cut curve for the eigenvalues of ϕ , but they locate the transition when this profile gets deformed with a dip at zero, instead of when it switches to two cut (if it ever does). This boundary line is absent in our phase diagram and in previous ones [6, 11, 12], and we find no evidence for such a transition or a new phase in this region of the phase diagram. As for the lack of scaling for the other phase boundaries, it is difficult to decide the cause, but it is disquieting

that their simulations sometimes depend on the initial condition, such as when they find hysteresis.

In the large N limit the model with $a = 0$ has a third order phase transition between disordered and non-uniform ordered phases [28, 29]. The disordered phase is described by a single connected eigenvalue distribution called a “one cut phase” distribution, whereas the ordered phase is described by an eigenvalue distribution split into two disconnected distributions centered on opposite values and called a “two cut phase” distribution. The transition occurs when the two cuts merge to become a single cut for $c = b^2/4N$. Figure 7 confirms numerically the convergence of the disordered/non-

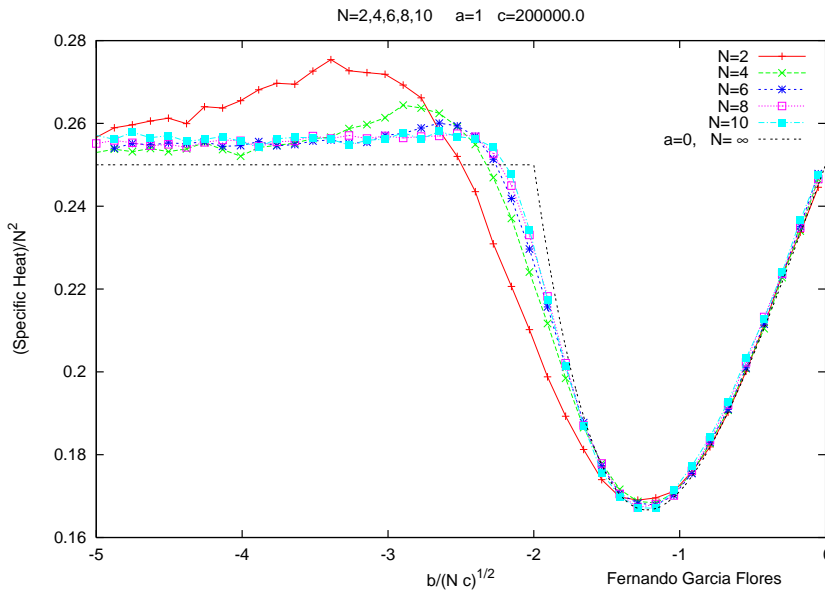


Figure 7: Plot of the specific heat at the disordered/non-uniform ordered transition for increasing N and its $N \rightarrow \infty$ limit, the exact pure potential model, given by Eq. (23).

uniform ordered transition towards this exact critical line of the pure potential model as the coupling is increased. The simulations of Panero [11, 12] confirm that this transition for the full model is indeed a one cut–two cut transition though the eigenvalue distribution now has a richer structure.

We expect that the existence of the cut transition of matrix models and of a triple point is a generic feature of fuzzy scalar field models, since all such models should reduce to a pure matrix model when the kinetic term becomes subdominant. This means that fuzzy scalar field models should generically have an exotic phase with spontaneously broken spacetime symmetry.

Numerically, it is not difficult to find the coexistence curve between the uniform ordered and

disordered phases which exist for low values of c . On the other hand, the coexistence curve between the two ordered phases is difficult to evaluate because it involves a jump in the field configuration and tunneling over a wide potential barrier.

In the current model the triple point is estimated to be located at

$$(\bar{b}_T, \bar{c}_T) = (-2.3, 0.52). \quad (32)$$

This is obtained by extrapolating the three coexistence lines till they meet. Surprisingly good agreement with this result was obtained in [7] by performing perturbation theory in the kinetic term, *i.e.* by expanding in the parameter a to second order. It is not however, totally clear that the triple point identified there coincides with the one here as a different scaling of the parameters was necessary, but the salient features are the same.

The position (31) where the curve (27) intersects the disordered /uniform order transition line suggests that the effect of the kinetic term is to push the transition, and hence the triple point, to larger negative values of b . This is a positive feature since it indicates that adding a higher derivative term to the model will allow one to tune the triple point to large coupling. The conjecture is that this will be sufficient to eliminate the UV/IR mixing problems [22] and recover the commutative theory with the correct fluctuations [23].

It still remains to be seen what thermodynamic limits can be drawn from the phase diagram and the scalings in each of the limits of the fuzzy sphere introduced in table 1: the ordinary sphere, the ordinary plane, and the Moyal plane.

To that end, we want to reexpress the positions of the coexistence curves (26,28,29) which depend on $a = 1$, b , c and N as a function of parameters well defined in the thermodynamic limit. These are the radius of the sphere R and the non-commutative parameter $\Theta = 2R^2/\sqrt{N^2 - 1}$ appearing in (6) and in the list of possible limits of the fuzzy sphere of Table 1, and r and λ appearing in the action (16,17).

Using the scalings of (25) and $N \simeq 2R^2/\Theta$, we find

$$\bar{b} = \frac{r\Theta^{3/2}}{2\sqrt{2}R}, \quad \bar{c} = \frac{\lambda\Theta}{48\pi}. \quad (33)$$

which can now be replaced in the algebraic fits for the coexistence curves to get

$$\text{Disorder/non-uniform:} \quad (\lambda\Theta) = 122 \left(-\frac{r\Theta^{3/2}}{R} \right) - 715 \quad (34)$$

$$\text{Disorder/uniform order:} \quad (\lambda\Theta) = 12.3 \left(-\frac{r\Theta^{3/2}}{R} \right) \quad (35)$$

$$\text{Uniform/non-uniform order:} \quad (\lambda\Theta) = 10.7 \left(-\frac{r\Theta^{3/2}}{R} \right) + 10.6 \quad (36)$$

$$\text{Triple point:} \quad \left(-\frac{r_T\Theta^{3/2}}{R} = 6.5, \lambda_T\Theta = 78.4 \right). \quad (37)$$

Since the phase boundary lines and the triple point all scale in the same way, it is not surprising to find that, out of the four physical quantities available, only two are independent: $r\Theta^{3/2}/R$ and $\lambda\Theta$. As a result there are not enough physical parameters to fix the limiting procedure. For instance, if the limiting space, represented by R and Θ , is fixed, one can still scale the field model parameters r and λ freely.

A Optimized algorithm for matrix models

We now present an improved Monte-Carlo scheme we used to speed up our simulations.

The probability transition function (denoted by **PTF** for short) of a Monte-Carlo algorithm $W_{f,i}$ from an initial state i with probability P_i to a final state f with probability P_f , must satisfy the detailed balance equation

$$P_i W_{f,i} = W_{i,f} P_f. \quad (38)$$

The Metropolis **PTF**

$$W_{fi} = \min \left[1, \frac{P_f}{P_i} \right] \quad (39)$$

is the best known example of one such, but another introduced in [32] is given by

$$W_{f,i}^B = w_{f,i} \min \left[1, \frac{P_f w_{i,f}}{P_i w_{f,i}} \right], \quad (40)$$

which is a generalization of the Metropolis **PTF** when $w_{f,i} \neq w_{i,f}$. In our case, we have selected the further generalization

$$w_{f,i} = \min \left[1, \frac{P_f}{p_i} \right], \quad (41)$$

which is equivalent to the Metropolis **PTF** using a different probability distribution p yet to be defined.

The Boltzmann probability density distribution $P(x)$ to find a configuration in the volume $(x, x + dx)$ is defined by

$$P(x) = \frac{1}{Z} e^{-S[x]}, \quad (42)$$

where $S[x]$ is the action or energy, and Z is the *partition function* which contains the whole relevant information of the system. In general, it is not possible to obtain an exact expression for the partition function analytically or numerically. The Monte-Carlo algorithm via the Metropolis **PTF** (38) is so important because it does not depend on Z .

With $\Delta S = S[x_f] - S[x_i]$, putting (42) in (39) gives us the **PTF** in terms of the Boltzmann probability density distribution (denoted **PDD** for short), that is

$$W_{f,i} = \min [1, e^{-\Delta S}]. \quad (43)$$

	$\Delta S \leq 0$	$\Delta S > 0$
$\Delta s \leq 0$	$W_{f,i}^B = \min [1, e^{-\Delta S + \Delta s}]$	$W_{f,i}^B = e^{-\Delta S + \Delta s}$
$\Delta s > 0$	$W_{f,i}^B = e^{-\Delta s}$	$W_{f,i}^B = \min [e^{-\Delta s}, e^{-\Delta S}]$

Table 2: Possible cases in the evaluation of the Probability Transition Function $W_{f,i}^B$.

In the same way as (42), we can associate a kind of energy $s(y)$ to the probability distribution p introduced in (41)

$$p(y) = \frac{1}{z} e^{-s[y]}. \quad (44)$$

Now, the new *Metropolis-Boghosian* **PTF** which comes from the equations (40), (41), (42) and (44) is given by

$$W_{f,i}^B = \min [1, e^{-\Delta s}] \min [1, e^{-\Delta S + \Delta s}] = \min [1, e^{-\Delta s}, e^{-\Delta S}, e^{-\Delta S + \Delta s}], \quad (45)$$

where $\Delta s = s[x_f] - s[x_i]$ is the equivalent of the ΔS defined above. All the possible cases for the **PTF** (45) are presented in the table 2.

We can ask why we might need the **PTF** (45) when we have a simpler function (43) already? When the evaluation of ΔS is quite simple, for instance for the Ising model, this methodology is counterproductive because more exponential functions must be evaluated. On the contrary, when the evaluation of ΔS is computationally very expensive, as the matrix models are, the **PTF** (45) avoids the evaluation of very improbable changes in the configurations due to the implementation of the filter Δs , which reduces the processing time.

Numerically, we do not want to evaluate both ΔS and Δs . If s is a good approximation of the effective potential created by S but simpler to evaluate then, we can use the Metropolis algorithm with the action s to refuse or accept the new configurations before the evaluation of ΔS (which is complicated to evaluate and only will take machine time).

In this section, we propose a variant calculation of **PTF** (45) shown in table 3, where we avoid the evaluation of ΔS when the previous evaluation of Metropolis algorithm with Δs refuses the attempt to change the configuration.

A.1 Relative error

The new **PTF**, denoted by $W_{f,i}^F$, can not satisfy the detailed balance equation (39). This fact introduces deviations in the probabilities, in exchange for a computational time reduction, since Δs will be chosen

i	$\Delta S \leq 0$	$\Delta S > 0$
$\Delta s \leq 0$	$W_{f,i}^F = \min [1, e^{-\Delta S + \Delta s}]$	$W_{f,i}^F = e^{-\Delta S + \Delta s} = \min [1, e^{-\Delta S + \Delta s}]$
$\Delta s > 0$	$W_{f,i}^F = e^{-\Delta s}$	$W_{f,i}^F = e^{-\Delta s}$

Table 3: Proposition for a faster Probability Transition Function.

	$\Delta S \leq 0$	$\Delta S > 0$
$\Delta s \leq 0$	0	0
$\Delta s > 0$	0	$\begin{cases} 0 & \text{if } \Delta S \leq \Delta s \\ 1 - e^{-\Delta S + \Delta s} & \text{if } \Delta S > \Delta s \end{cases}$

Table 4: Relative error (46) between the probability transition functions, $W_{f,i}^B$ and $W_{f,i}^F$.

simple to calculate. Anyway, we will make sure to keep under control the error introduced by this breaking of the detailed balance equation.

In accordance to this, the relative error between $W_{f,i}^B$ and $W_{f,i}^F$ is defined as

$$\text{err} = \left| 1 - \frac{W_{f,i}^B}{W_{f,i}^F} \right|, \quad (46)$$

and its values are shown in table 4. As we can see in that table, only the case $\Delta S > \Delta s > 0$ presents a relative error different from zero. This error goes to zero when $\Delta S \gtrsim \Delta s$ and it goes to one when $\Delta S \gg \Delta s$. Similarly, when $\Delta S \gg 1$ we can almost take for granted the rejection of the new configuration by Metropolis. Thus, the introduction of the **PTF** $W_{f,i}^F$ is very convenient to estimate the **PTF** given by (43) breaking the detailed balanced equation, where we only expect a tolerably small deformation in the averages (specifically in regions with low probability) with respect to the averages obtained from the **PTF**'s (43) and (45).

In our experience, we can obtain a better approximation when we replace $\Delta s \rightarrow (\Delta S)'$ only in the case $\Delta S > \Delta s > 0$. The prime indicate the difference of energy obtained by Metropolis one step before under the condition $\Delta S > \Delta s > 0$. In that way, the algorithm has a kind of ‘‘auto-regulation’’ which reduces the deviation of the averages with respect to the **PTF** which obeys the detailed balance equation. With this auto-regulation we only update the energy reference level.

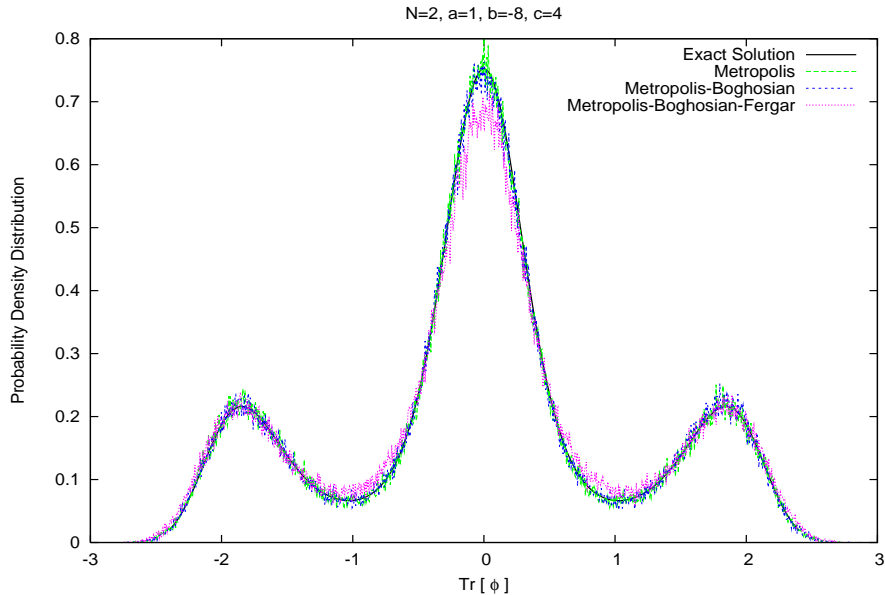


Figure 8: The **PDD**'s obtained by different methods for $N = 2$.

A.2 Application to the fuzzy scalar field model

We can now adapt this scheme to the matrix model (16) we are considering in this article. A finite variation of the action, from a configuration ϕ to a configuration $\phi + \bar{\phi}$ is defined by $\Delta S = S[\phi + \bar{\phi}] - S[\phi]$, where $\bar{\phi}$ must be a Hermitian matrix. The evaluation of $(\Delta S)_{\mu\nu}$ for the ϕ^4 matrix model for a single entry (μ, ν) , involves the evaluation of a cubic polynomial in the matrix. This is a highly non-local function which causes the main slow-down in the code.

Figure 8 shows a comparison for the same set of internal parameters (Monte Carlo time, thermalization time, decorrelation time, etc.), at a collapsed point $(\bar{b}, \bar{c}) = (-2^{3/2}, 1)$ from the phase diagram -Figure 6- corresponding to the non-uniform ordered phase, between the results obtained by direct integration (explained in Section 5.1), and the Monte Carlo simulations via either of the three probability transition functions presented above: Metropolis, Metropolis-Boghosian, and Metropolis-Boghosian-Fergar (the one in Table 3). The small deviations (noise) of the Monte-Carlo simulations with respect to the direct integration are a normal effect of the Monte Carlo simulations and can be reduced by increasing the number of samples produced by the code.

Going back to the choice of the filter s introduced in (44), we want a function that incorporates the main features of S but is easier to evaluate.

We can notice that the action (16) for a fixed entry (μ, ν) of the matrix ϕ correspond to a quartic

polynomial in the entry $\phi_{\mu\nu}$, thus

$$S_{\mu\nu} = C\phi_{\mu\nu}^4 + B\phi_{\mu\nu}^2 + A,$$

where the coefficients A , B and C depend on the rest of the entries in the matrix. In that sense, we propose

$$s_{\mu\nu} = C'\phi_{\mu\nu}^4 + B'\phi_{\mu\nu}^2 + A', \quad (47)$$

where A' , B' and C' are constant coefficients. Thus, $s_{\mu\nu}$ goes to $S_{\mu\nu}$ when $\{A', B', C'\} \rightarrow \{A, B, C\}$. We will obtain a better concordance between both ΔS and Δs by choosing a set of parameters $\{A', B', C'\}$ close to the non-primed parameters. As a first approximation, we took

$$\{A', B', C'\} = \begin{cases} \{0, b, c\} & \text{if } \mu = \nu \\ \{0, 0, c\} & \text{if } \mu \neq \nu \end{cases}$$

where b and c are respectively the bare mass and interaction parameters of the model (16). For simplicity we have fixed $A' = 0$ but in general, we can use any other real number and it will not affect Δs . This set of primed parameters for s , was chosen to contain the most basic information of the full model S .

At the end of section 3, we have shown that the action (16) has two symmetric minima with respect to the trace. Those minima are located in $\text{Tr}[\phi] = \pm N\sqrt{-\frac{b}{2c}}$. Thus, *we can consider that every single diagonal entry in the matrix contributes to the trace minima with $\phi_{\mu\mu} = \pm\sqrt{-\frac{b}{2c}}$, where $(\mu = 1, 2, \dots, N)$.* A simple function of $\phi_{\mu\mu}$ with the same set of minima has been given in the equation (47) with the parameters ($A' = 0, B' = b, C' = c$).

For non-diagonal entries, we have observed that their probability distribution is around zero. Thus, it is enough to consider the function (47) with the parameters ($A' = 0, B' = 0, C' = c$).

A.3 The algorithm

The algorithm is basically the same as the usual Metropolis algorithm although with some adaptations to the current setting. In the figure 9 we show the flow chart for the implementation of the new method that we have proposed.

Internal variables in the flow chart 9.

- x and x' : random numbers uniformly distributed in the open interval $(0, 1)$.
- $\text{Metropolis}(\Delta f)$: indicates the Metropolis algorithm using the difference of energy

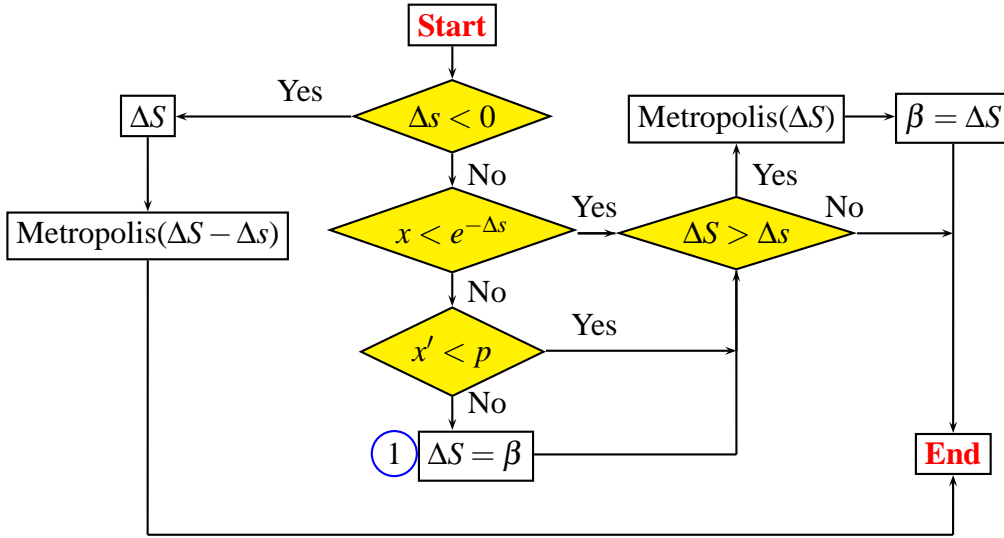


Figure 9: Flow chart of the Optimized Monte–Carlo method.

- Δf .
- β : represents the difference of the energy from a Monte–Carlo step which had been evaluated before.
- p : ratio of implementation of the new method with respect to the standard one.
- **1**: part of the subroutine where we avoid to evaluate ΔS .

In the flow chart presented above, we have emphasized with **1**, the step in the simulation where we avoid the evaluation of ΔS . This would seem to be insufficient to reduce in a significant way the processing time but it is not true at all. The number of times that the algorithm passes through **1** divided by the total number of times that the Modified Metropolis Algorithm (**MMA** for short) has been used, will be an estimation of the efficiency of the new method with respect to the Usual Metropolis Algorithm (**UMA** for short).

Let us first define an efficiency parameter for our **MMA** to compare it to the **UMA**. If T_{MC} is the Monte Carlo time to run the simulation for $N \times N$ Hermitian matrices under the model (16), and τ the number of times that the algorithm passes through the new feature **1**, then

$$\text{eff} = \frac{\tau}{N^2 T_{MC}}, \quad (48)$$

defines the efficiency of the modified algorithm. In particular, if t_{full} is the time for a run with a **UMA**, which is without our routine **1** and t_{gb} the time with it then, we have $t_{\text{gb}} \approx (1 - \text{eff}) t_{\text{full}}$.

Remember that the figure 9 only represents one attempt to switch one entry and, if β has been

updated then it must be saved for the next one.

The modification of the Metropolis algorithm presented in this chapter allows us to simulate matrix models with a decrease of the calculation time with respect to the usual method. The explicit breaking of the detailed balance equation by our proposition involves a systematic error which we can keep under control at any time.

A.4 The optimized Metropolis method

As a second part, we present the results obtained with the optimized Metropolis method. As explained in section A.2, this method was successfully tested in the lowest dimensional $N = 2$ case.

As we saw in the figure 9, the Modified Metropolis Algorithm (or **MMA**) had to evaluate three exponential functions compared with the Usual Metropolis Algorithm (or **UMA**) where we only have to evaluate one. Thus, when the efficiency eff defined in (48) is too small, it could be better to use the **UMA**. This happens for instance, in the *disordered phase*: the difference in processing time between **UMA** and **MMA** is not appreciable³. Even worse, the processing time in **MMA** could be a little bigger in that phase.

It is not the same for the other two phases where tunneling plays an important role. There the efficiency eff goes to one and the **MMA** is greatly more efficient⁴.

To keep under control the *relative error* when eff is close to one, we have to adjust the p ratio. Thus, $p \approx 0$ means a fast run, but could present a considerable relative error. At the other extreme, when $p \approx 1$, the run will be slow but the relative error will be very small. We have to look for a balance between accuracy and speed. We have set p between 0.55 and 0.70 but it is also possible to set it dynamically.

As an example, in the figure 10, we show the behavior of the processing time per configuration with respect to the matrix size obtained by means of the usual Metropolis algorithm for some given processor⁵ when $a = 1$, $\bar{b} = -4$ and $\bar{c} = 0.10$ which corresponds to the *uniform ordered phase* where we expect some gain. And indeed, the best fit for this curve $\text{time} = (1.49 \pm 0.02 \times 10^{-6})N^2 + (3.18 \pm 0.02 \times 10^{-8})N^4$ s grows like N^4 .

³They have approximately the same velocity of processing because a large percent of attempts will be in the range of fluctuations of s .

⁴In these phases, the new method is faster than the old one because a large percentage of attempts could be out of the range of fluctuations of s , thus avoiding the evaluation of ΔS .

⁵In this example we have used a *Mobile Intel(R) Pentium(R) III CPU - M 800MHz, 369.10Mb RAM*. On gcc-4.0.2 2005-10-01, Ubuntu, kernel 2.6.12-10-386. Kubuntu 5.10 Breezy Badger.

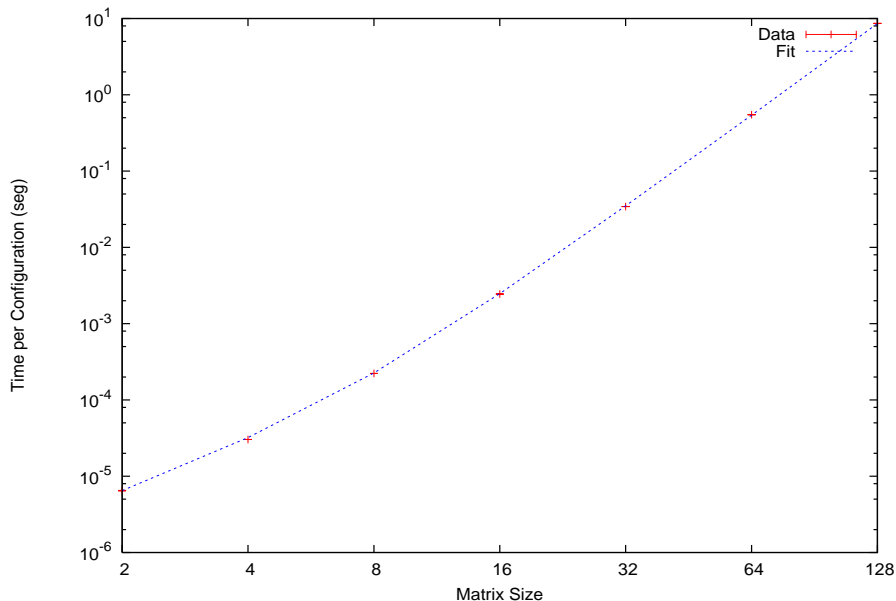


Figure 10: Processing time per configuration for the **UMA**.

Starting from a random configuration, it can be thermalized or decorrelated using the **MBF** method described by Table 3, then we can use the usual Metropolis algorithm to evaluate the probability of transition between the old configuration and this new sample obtained from **MBF**. Doing this, we save processing time and, at the same time, we do not introduce any systematic error because the usual Metropolis algorithm will reject or accept the new configuration which only contains the statistical error.

References

- [1] J. Hoppe, MIT Ph.D. thesis (1982); J. Hoppe, *Elem. Part. Res. J. (Koyoto)* **80** 145 (1989).
H. Grosse and P. Presnajder, *Lett.Math.Phys.* **33**, 171 (1995); H. Grosse, C. Klimčík and P. Presnajder, *Commun.Math.Phys.* **178**,507 (1996); **185**, 155 (1997); H. Grosse and P. Presnajder, *Lett.Math.Phys.* **46**, 61 (1998) and ESI preprint, (1999); H. Grosse, C. Klimčík, and P. Presnajder, hep-th/9602115 and *Commun.Math.Phys.* **180**, 429 (1996); H. Grosse, C. Klimčík, and P. Presnajder, in *Les Houches Summer School on Theoretical Physics*, 1995, hep-th/9603071. S. Baez, A. P. Balachandran, S. Vaidya and B. Ydri *Commun.Math.Phys.* **208**, 787-798 (2000); . P. Balachandran, T.R.Govindarajan and B. Ydri, *Mod.Phys.Lett.* **A15** 1279

- (2000); G.Alexanian, A.P.Balachandran, G.Immirzi and B.Ydri *J.Geom.Phys.* **42** 28–53 (2002);
Badis Ydri hep-th/0110006.
- [2] J. Medina, W. Bietenholz, F. Hofheinz and D. O’Connor, PoS **LAT2005**, 263 (2006) [arXiv:hep-lat/0509162].
- [3] H. Steinacker, *JHEP* **04** (2004) 077 [arXiv:hep-th/0501174]; H. Steinacker, [arXiv:hep-th/0511076v1].
- [4] J. Ambjorn and S. Caterall, *Phys. Lett. B* **549** (2002) 253 [arXiv:hep-lat/0209106].
- [5] W. Bietenholz, F. Hofheinz, and J. Nishimura, *JHEP* **0406** (2004) 042 [arXiv:hep-th/0404020].
- [6] X. Martin, *JHEP* **0404**, 077 (2004) [arXiv:hep-th/0402230].
- [7] D. O’Connor and C. Saemann, *JHEP* **0708** (2007) 066 [arXiv:0706.2493 [hep-th]].
- [8] D. O’Connor and C. Saemann, arXiv:0709.0387 [hep-th].
- [9] H. Steinacker, *JHEP* **0503** (2005) 075 [arXiv:hep-th/0501174].
- [10] F. García Flores, D. O’Connor and X. Martin, PoS **LAT2005** (2006) 262 [arXiv:hep-lat/0601012].
- [11] Marco Panero. *JHEP* **0705** (2007) 082 [arXiv:0608202[hep-th]].
- [12] M. Panero, *SIGMA* **2** (2006), 081 [arXiv:hep-th/0609205].
- [13] C. R. Das, S. Digal and T. R. Govindarajan, arXiv:0706.0695 [hep-th].
- [14] A. P. Balachandran, B. P. Dolan, J. H. Lee, X. Martin and D. O’Connor, *J. Geom. Phys.* **43**, 184 (2002) [arXiv:hep-th/0107099].
- [15] B.P. Dolan and D. O’Connor, *JHEP* **0310** (2003) 060 [arXiv:hep-th/0306231].
- [16] Jurgen Jost, “Riemannian Geometry and Geometric Analysis”. *Spring-Verlag 3rd edition*. Berlin, 2002; Charles W. Misner, Kip S. Thorne, John Archibald Wheeler, “Gravitation”. *W.H. Freeman*. New York, 1970.
- [17] G. Landi, arXiv:hep-th/9701078.
- [18] M. R. Douglas and N. A. Nekrasov, *Rev. Mod. Phys.* **73**, 977 (2001) [arXiv:hep-th/0106048].
- [19] J. Madore, *Class. Quant. Grav.* **9** (1992) 69.
- [20] J. Glimm and A.M. Jaffe, *Phys. Rev. D* **10** (1974) 536; J. Glimm and A.M. Jaffe, and T. Spencer, *Comm. Math. Phys.* **45** (1975) 203.

- [21] W. Loinaz and R.S. Willey, *Phys. Rev. D* **58** (1998) 076003 [arXiv:hep-lat/9712008]; D. Lee, *Phys. Lett. B* **439** (1998) 85 [arXiv:hep-th/9811117].
- [22] C.-S. Chu, J. Madore and H. Steinhacker, *JHEP* **0108** 038 (2001); B.P. Dolan, D. O’Connor and P. Prešnajder, *JHEP* **0203** 013 (2002).
- [23] B.P. Dolan, D. O’Connor, and P. Presnajder, *JHEP* **03** (2002) 013 [arXiv:hep-th/0204219].
- [24] N. Metropolis, A. Rosenbluth, M. Rosebluth, A. Teller, and E. Teller, *J. Chem. Phys.* **21**, 1087 (1953).
- [25] David Landau, Kurt Binder, “A Guide to Monte Carlo Simulations in Statistical Physics”. *Cambridge University Press* August (2000); M. E. J. Newman, G. T. Barkema, “Monte Carlo Methods in statistical Physics”. *Oxford University Press* August (2001).
- [26] J. Shao and D. Tu, “The Jackknife and Bootstrap,” (Springer, New York, 1995).
- [27] William H. Press, Brian P. Flannery, Saul A. Teukolsky, William T. Vetterling, “Numerical Recipes in Fortran”. *Cambridge University Press; 2 edition* January, (1992).
- [28] Y. Shimamune, *Phys. Lett. B* **108** (1982) 407.
- [29] E.Brézin, C. Itzykson, G. Parisi and J. B. Zuber. *Comm. Math. Phys.* **59**, 35 (1978); P. Di Francesco, P. Ginsparg, J. Zinn-Justin. arXiv:hep-th/9306153; Pavel Bleher, Alexander Its. arXiv:math-ph/0201003.
- [30] F. G. Flores, “Simulación de un campo escalar sobre una esfera fuzzy”, PhD tesis published at Cinvestav, México (2008).
- [31] J. Medina, W. Bietenholz and D. O’Connor, “Probing the fuzzy sphere regularisation in simulations of the $3d \lambda \phi^4$ model,” arXiv:0712.3366 [hep-th].
- [32] Bruce M. Boghosian. *Physical Review E* **60** 1189-1194 (1999).